Modeling of surface structure formation after laser irradiation

J. KAUPUŽS
Institute of Mathematical Sciences and Information Technologies
University of Liepaja
14 Liela Street
Liepaja LV-3401
LATVIA
kaupuzs@latnet.lv

SH. E. GUSEYNOV
Institute of Mathematical Sciences and Information Technologies
University of Liepaja
14 Liela Street
Liepaja LV-3401
LATVIA
sh.e.guseinov@inbox.lv

J. RIMSHANS
Institute of Mathematical Sciences and Information Technologies
University of Liepaja
14 Liela Street
Liepaja LV-3401
LATVIA
rimshans@latnet.lv

A. MEDVID'
Institute of Technical Physics
Riga Technical University
14 Āzenes Street
LV-1048, Riga
LATVIA
medvids@latnet.lv

Abstract: The Stefan problem in a semi-infinite media under laser irradiation is considered. It is related to the melting and solidification processes, resulting in certain surface structure after the solidification. A simple model, as well as a more sophisticated one is proposed to describe this process. The latter model allows us to calculate the surface profile by solving a system of two nonlinear differential equations, if the shape of the solid-liquid interface is known. It has to be found as a solution of two-phases Stefan problem. The results of example calculations by the fourth-order Runge-Kutta method are presented, assuming that the solid-liquid interface has a parabolic shape. The calculated crossection of the surface structure shows a characteristic cone in the center, in agreement with experimental observations.

Key–Words: Stefan problem, Greens functions, laser irradiation, surface structure, differential equations, Runge-Kutta method, Euler-Lagrange equation

1 Introduction

Recently, a problem of a controllable, direct laser fabrication of sharp conical structures on silicon thin films has attracted a significant interest [1, 2, 3]. The laser irradiation causes melting of the material, which is followed by the solidification after the laser pulse. If the solid has a smaller density than the liquid, then the melt is pushed upwards at the end phase of this process, resulting in a characteristic conic shape of the surface. Here we propose a mathematical model to describe this process. We start with a simple model, which is similar (but not identical) to the one considered in [1], and then refine it. The solution of our equations shows how the formed surface profile depends on the shape of the solid–liquid interface.

2 The Stefan problem

2.1 One–phase problem

We consider the heat conduction in a semi-infinite media in a process of laser irradiation. The laser beam is perpendicular to the media surface, and its intensity depends on the distance r from the center. In this case, the temperature distribution $T(r,z,t)$ has a cylindric symmetry, where r is the distance from the symmetry axis, z is the distance from the media surface and t is time. Another situation takes place in the experiments discussed in Sec. 4, where the absorption of the laser power is larger and the melting temperature is lower in some very small local regions with a high impurity concentration. Assuming the cylindric symmetry for the local impurity concentration and the local temperature distribution (or for the shape of the solid–liquid interface in the two–phases Stefan problem), our description can be applied also to these experiments.

In the case where no melting of the material is reached, the heat conduction equation reads

$$\frac{\partial T}{\partial t} = \nabla(\sigma \nabla T) + g \,, \tag{1}$$

where $\sigma = \kappa/(\rho c)$ is the heat diffusion coefficient and $g = g(r,z,t) = Q/(\rho c)$ is the source function. Here κ is the coefficient of heat conduction, ρ is the density of material, c is the specific heat, and Q is the laser heat source. Neglecting the heat exchange between the heated material and surrounding media, the initial and boundary conditions are

$$T(r,z,0) = T_0 \,, \tag{2}$$

$$\left.\frac{\partial T(r,z,t)}{\partial z}\right|_{z=0} = 0 \,, \tag{3}$$

where T_0 is the initial temperature.

ISBN: 978-960-474-268-4

In a special case, where σ is constant, Eq. (1) reduces to

$$\frac{\partial T}{\partial t} = \sigma \, \Delta T + g \; . \qquad (4)$$

In this case the solution can be easily represented by the heat Greens function $G(r,t)$ [4], which is the spherically–symmetric solution of the heat conduction equation in infinite space with a point–like source

$$\frac{\partial G}{\partial t} = \sigma \, \Delta G + \delta(\mathbf{x})\delta(t) \; , \qquad (5)$$

and initial condition $G(r,0) = 0$. Here $\delta(\mathbf{x})$ is the three–dimensional delta function. To construct the solution, first we map the actual problem in the semi-infinite space to the one in infinite space by adding the second heat source, which is the mirror–symmetric reflection of the original source with respect to the $z = 0$ plane. In this case the boundary condition (3) is satisfied automatically. The total heat source is represented as a superposition of the point–like sources, and, due to the linearity of the equation (4), the solution for $Y(r,z,t) = T(r,z,t) - T_0$ is the superposition of the corresponding Greens functions:

$$Y(r,z,t) = 2 \int_0^t d\tau \int_0^\infty dx \int_0^\infty r' dr' \int_0^\pi d\varphi \times g(r',x,\tau)$$
$$\times \Big[G\left(\sqrt{r^2 + 2rr'\cos\varphi + r'^2 + (x-z)^2}, t-\tau \right) \qquad (6)$$
$$+ \, G\left(\sqrt{r^2 + 2rr'\cos\varphi + r'^2 + (x+z)^2}, t-\tau \right) \Big] \; .$$

2.2 Two–phases problem

Consider a case where there are two phases, solid and liquid, but there are no differences between these phases in the context of the heat conduction. However, certain melting latent heat L_m is necessary to transform from solid to liquid. Such a situation can be modeled by setting $\widetilde{c} = c + \delta(T - T_m)L_m$ instead of specific heat c, as it has been done, e. g., in [1]. Indeed, in this case one needs to input the specific energy equal to L_m to increase the temperature from $T_m - \delta T$ to $T_m + \delta T$ at $\delta T \to 0$. (This energy is related to the jump in enthalpy ΔH, i. e., $\Delta H = \Delta U + P\Delta V$, where ΔU is the jump in the internal energy, P is the pressure, and ΔV is the change in volume.) In such a way, the heat conduction equation reads

$$\frac{\partial T}{\partial t} = \nabla(\widetilde{\sigma}\nabla T) + \widetilde{g} \; , \qquad (7)$$

where

$$\widetilde{\sigma} = \frac{\sigma}{1 + \delta(T - T_m)L_m/c} \; , \qquad (8)$$

$$\widetilde{g} = \frac{g}{1 + \delta(T - T_m)L_m/c} \; . \qquad (9)$$

However, we do not take $\widetilde{\sigma}$ in front of ΔT to obtain simplified equation of the type (4), as it has been actually done in [1], since $\widetilde{\sigma}$ is not a constant. Eq. (7) might be useful in numerical solution of the problem, approximating the delta function by a peak of finite width, and determining the solid–liquid interface on which $T = T_m$ holds.

3 The surface structure

Let us assume that liquid phase has a larger density ρ_l than that of the solid phase ρ_s, i. e., $\rho_l > \rho_s$. In this case certain structure forms on the surface in the solidification process after laser pulse. A simple model to describe this phenomenon has been already introduced in [1]. As a first approximation, we propose a similar model (model A). Namely, it is assumed in model A that the liquid surface is always flat. Distinct from [1], our model is formulated for an arbitrary shape of the solid–liquid interface. Later, we will consider refined models (models B and C), where the curvature of the liquid surface is taken into account, assuming that the liquid is attached to the top of the molten area due to the capillarity forces.

3.1 Model A

The model A is illustrated in Fig. 1, where the crossection of the considered structure of cylindric symmetry is shown. Here we have assumed for illustration that the crossection of the solid–liquid interface has a parabolic shape, as shown by solid curves in Fig. 1. At the initial stage (Fig. 1, top), the surface of the melt (horizontal dashed line) with radius R_0 lies below the initial surface of the solid (horizontal solid lines) because $\rho_l > \rho_s$. In the following solidification process, the solid–liquid interface moves up. Since $\rho_l > \rho_s$, the liquid phase and the newly formed solid surface are pushed up in this process (Fig. 1, middle).

Let us denote by $h(r,R)$ the depth of the molten are of radius R at a distance r from the center (see Fig. 1 top). Considering an infinitesimal shift in phase boundaries, such that $R \to R + dR$ (with $dR < 0$), the solid–liquid interface being shifted up by $\delta h(r,R)$, we have

$$\delta h(r,R) = h(r,R) - h(r,R+dR) + dH$$
$$= -\frac{\partial h(r,R)}{\partial R} dR + dH + O\left((dR)^2\right) \; , \qquad (10)$$

where dH is the shift of the solid surface, as shown in Fig. 1. According to the mass conservation law, we

ISBN: 978-960-474-268-4

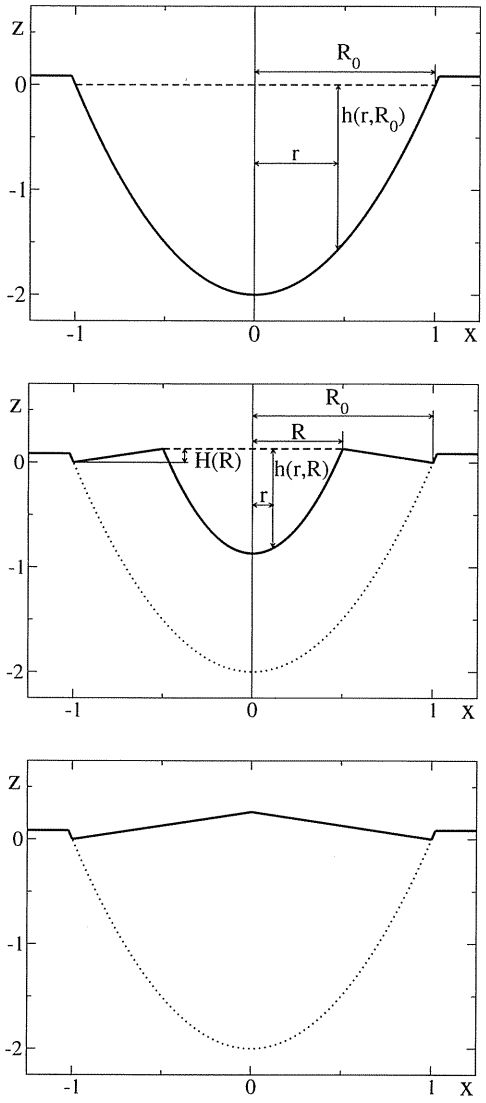

Figure 1: Different stages of the formation of solid surface after the laser pulse: initial molten area of a parabolic crossection (top), intermediate stage (middle), and final surface structure (bottom). The dashed horizontal line shows the liquid surface. The solid–liquid interface is represented by that part of the solid curve, which lies at distances $r < R$ from the center, the remaining its part being the external solid surface. Here R is the current radius of the molten area with $R = R_0$ at the beginning, $h(r, R)$ is the depth of the molten area and $H(R)$ is the height of the formed surface profile. The dotted curve indicates the initial location of the solid–liquid interface.

have

$$\pi R^2 dH = \int_0^R \Big(\delta h(r,R) - \widetilde{\delta h}(r,R)\Big)\, 2\pi r dr \ , \quad (11)$$

where

$$\widetilde{\delta h}(r,R) = \frac{\rho_s}{\rho_l}\, \delta h(r,R) \quad (12)$$

is the width of the liquid phase layer, measured along z axis at a distance r from the center, which becomes solid layer of the width $\delta h(r, R)$. According to (12) and (10), Eq. (11) becomes

$$R^2 dH = 2\mu \int_0^R \delta h(r,R) r dr$$

$$= \mu \left\{ R^2 dH - 2\, dR \int_0^R \frac{\partial h(r,R)}{\partial R} r dr \right\} , \quad (13)$$

where $\mu = 1 - (\rho_s/\rho_l)$. It leads to the differential equation

$$\frac{dH}{dR} = -\frac{2\mu}{(1-\mu)R^2} \int_0^R \frac{\partial h(r,R)}{\partial R} r dr \ . \quad (14)$$

The initial condition is $H(R_0) = 0$. From this equation we can calculate the surface profile after the solidification, represented by H as a function of R, if $h(r, R)$ is known, i. e.,

$$H(R) = \frac{2\mu}{1-\mu} \int_R^{R_0} \left(\frac{1}{x^2} \int_0^x \frac{\partial h(r,x)}{\partial x} r dr \right) dx \ . \quad (15)$$

The function $h(r, R)$ describes the shape of the solid–liquid interface. In reality, it should be determined by solving the related Stefan problem for the two–phase system. For an illustration, we approximate it by a parabola

$$h(r,R) = \alpha R \left[1 - \left(\frac{r}{R} \right)^2 \right] \ . \quad (16)$$

In this case, the solution is

$$H(R) = \frac{3\mu\alpha}{2(1-\mu)} \left(R_0 - R \right) , \quad (17)$$

providing a conic surface structure, shown in Fig. 1 (bottom) at the shape parameter $\alpha = 2$. The relative density difference μ has been taken $\mu = 0.08$, as in [1].

ISBN: 978-960-474-268-4

For a general $h(r, R)$, the mass conservation during the solidification process implies that the relation

$$\int_0^{R_0} H(R) R\, dR = \frac{\mu}{1-\mu} \int_0^{R_0} h(R, R_0) R\, dR \qquad (18)$$

must hold. It is easy to verify that it holds for (16) and (17).

3.2 Model B

In the model B, the shape of the liquid surface is approximated by a parabola (see Fig. 2)

$$f(r, R) = f_0 \left\{ 1 - \left(\frac{r}{R} \right)^2 \right\} \qquad (19)$$

with parameter $f_0 = f_0(R)$ found self consistently from the material (mass) conservation law. In this model, deviation of the liquid surface $f(r, R)$, as well as the depth of the molten area $h(r, R)$ are measured from the level of the solidification surface $H(R)$, as indicated in Fig. 2 (top left). As before, R denotes the current radius of the molten area, its initial value being R_0. Note that $f(r, R)$ is assumed to be positive, if the liquid surface is curved up, and negative – if it is curved down. The variation of this picture at different solidification steps is shown in Fig. 2.

Let us introduce the angles φ, γ, and θ, measuring the slopes

$$\tan\varphi = \frac{dH}{dR}\,, \qquad (20)$$

$$\tan\gamma = -\left.\frac{\partial h(r, R)}{\partial r}\right|_{r=R}\,, \qquad (21)$$

$$\tan\theta = \left.\frac{\partial f(r, R)}{\partial r}\right|_{r=R}\,. \qquad (22)$$

The variation of the surface profile at each step $R \to R + dR$ (with $dR < 0$) is found assuming that certain layer of width $\tilde{\delta} h(r, R)$ (measured along z axis) expands in the direction perpendicular to the solid–liquid interface, becoming solid layer of the width $\delta h(r, R) = (\rho_l/\rho_s)\tilde{\delta} h(r, R)$. It implies the relation

$$\frac{\tan(\gamma - \theta)}{\tan(\gamma - \varphi)} = 1 - \mu\,, \qquad (23)$$

Further on, we use also the relations between small increments (according to the definitions given)

$$\frac{\partial h(r, R)}{\partial R} dR = dH - \delta h(r, R) \qquad (24)$$

$$df(r, R) = df_0 \left(1 - \left(\frac{r}{R} \right)^2 \right) + \frac{2r^2}{R^3} f_0(R) dR \qquad (25)$$

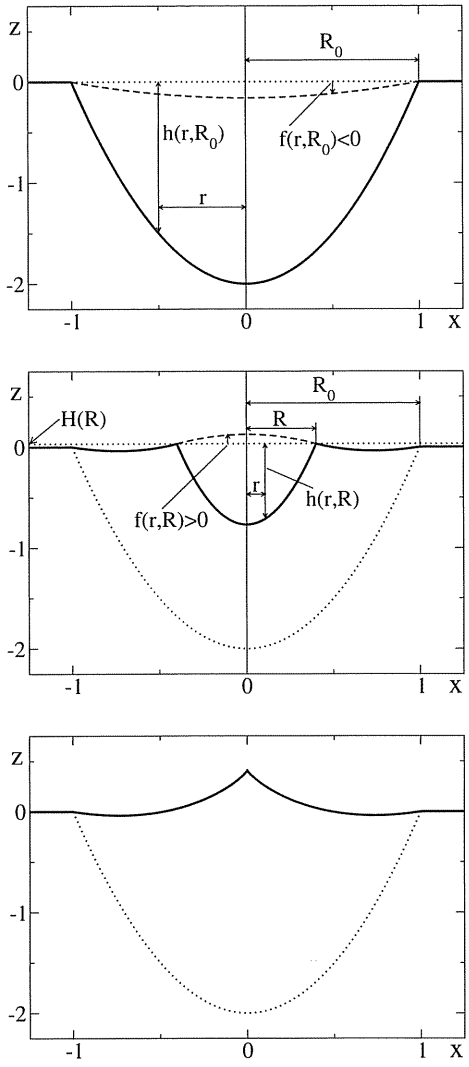

Figure 2: Different stages of the formation of solid surface after the laser pulse: initial molten area of a parabolic crossection (top), intermediate stage (middle), and final surface structure (bottom). The solid–liquid interface is represented by that part of the solid curve, which lies at distances $r < R$ from the center, the remaining its part being the external solid surface. Here R is the current radius of the molten area with $R = R_0$ at the beginning. The dotted curve indicates the initial location of the solid–liquid interface. The dashed curve shows the liquid surface, described by the deviation $f(r, R)$ from the horizontal dotted line. This line indicates the height $H(r)$ of the formed surface profile at the distance R from the center. The depth of the molten area $h(r, R)$ also is measured from this dotted line.

ISBN: 978-960-474-268-4

and the mass conservation law

$$\pi R^2 dH + 2\pi \int_0^R df(r,R) r dr = 2\pi\mu \int_0^R \delta h(r,R) r dr \ . \tag{26}$$

Summarizing the relations of this subsection, the formation of surface structure in the refined model B is described by the system of two nonlinear differential equations

$$\begin{aligned} \frac{df_0}{dR} &= -\frac{2f_0}{R} - 2(1-\mu)Q(f_0,R) \\ &- \frac{4\mu}{R^2}\int_0^R \frac{\partial h(r,R)}{\partial R} r dr \end{aligned} \tag{27}$$

$$\frac{dH}{dR} = Q(f_0,R) \ , \tag{28}$$

where

$$\begin{aligned} &Q(f_0,R) \\ &= \tan\left\{\gamma(R) - \arctan\left(\frac{\tan(\gamma-\theta(f_0,R))}{1-\mu}\right)\right\} \end{aligned} \tag{29}$$

with

$$\gamma(R) = -\arctan\left(\left.\frac{\partial h(r,R)}{\partial r}\right|_{r=R}\right) \tag{30}$$

$$\theta(f_0,R) = -\arctan\left(\frac{2}{R} f_0(R)\right) \ . \tag{31}$$

The equations (27) and (27) have to be solved with the initial conditions

$$f_0(R_0) = -\frac{4\mu}{R_0^2}\int_0^{R_0} h(r,R_0) r dr \tag{32}$$

$$H(R_0) = 0 \tag{33}$$

starting at $R = R_0$ and ending at $R = 0$. The initial condition (32) represents the requirement that the initial volume of the liquid phase differs by factor ρ_s/ρ_l from the corresponding volume of the solid before melting.

The final volume of the solid has to be the same as before the melting process. This mass conservation law in the model B has a simple form

$$\int_0^{R_0} H(r) r dr = 0 \ . \tag{34}$$

We have verified that the mass conservation law (34) holds with a high numerical accuracy in our calculations.

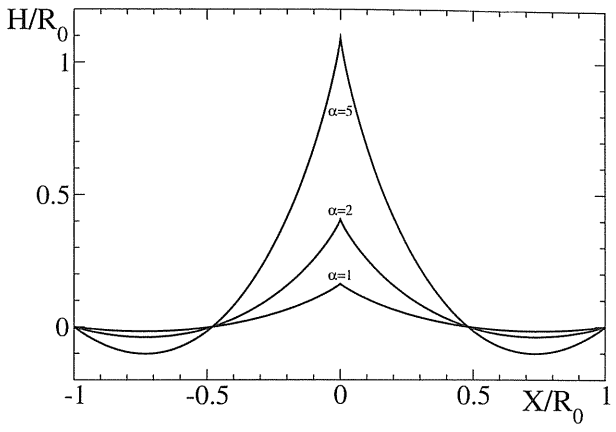

Figure 3: The profile (crossection) of the surface structure after the solidification for various values of the parameter α.

To see what can be obtained from our refined model B, the results of the numerical solution (by fourth–order Runge–Kutta method [5]) are plotted in Fig. 3, assuming that the solid–liquid interface is given by the same parabola (16) with $\alpha = 2$ as in the example considered before (Sec. 3.1). We have also set $\mu = 0.08$ in this case. As compared to model A (Fig. 1), the actually obtained shapes of the surface structure in Fig. 3 are better consistent with experimentally observed ones in [1]. Namely, the sharp dropping down at the periphery (at $R \approx R_0$), seen in Fig. 1 (bottom), is an artifact not observed experimentally (see Fig. 1 in [1]). The experimental profile goes smoothly downwards at the periphery, providing a direct evidence that the liquid phase initially is attached at the top of the molten area, as assumed in model B.

3.3 Model C

In this section, we will consider a real shape of the liquid surface instead of the parabolic approximation (19), in accordance with the free energy minimum principle. The corresponding refined model is further called model C. In the following, we will see that the real shape is spherical, so that the parabolic form (19) is a good approximation for a relatively flat surface, and the model B is certain limit case of model C. The latter property is very useful in verification of the derived expressions.

The liquid surface can be characterized by certain free energy per unit area. Further on, we will neglect gravity effects, which may change significantly the equilibrium shape of macroscopic liquid objects, like droplets, but are negligible in a micrometer scale. In our case, the free energy minimum corresponds to

ISBN: 978-960-474-268-4

the minimal surface area S at a given liquid volume V and a fixed radius R of the molten area. Assuming that the shape of the liquid surface at a given R is described by some unknown function $f(r)$, measuring a deviation from the $z = H(R)$ plane, we have

$$S = 2\pi \int_0^R \sqrt{1+f'^2}\, r dr \,, \qquad (35)$$

$$\widetilde{V} = 2\pi \int_0^R f(r)\, r dr \,. \qquad (36)$$

Here $f' = df/dr$ and $\widetilde{V} = V - \bar{V}$, where $\bar{V}$ is the volume of the spatial region between the solid–liquid interface and the $z = H(R)$ plane. The condition $f(R) = 0$ holds by definition of $f(r)$. Besides, we have $f'(0) = 0$ due to the symmetry of the problem. Note that the constant $\widetilde{V}$ can be positive or negative depending on that whether the liquid surface is curved up or down.

Using the Lagrange variational method, the problem reduces to finding of such function $f(r)$, which minimizes the functional

$$\mathcal{L}(f) = \int_0^R \left(\sqrt{1+f'^2} + \lambda f(r)\right) r dr \,, \qquad (37)$$

where λ is the unknown Lagrangian multiplier, chosen in such a way to satisfy the condition (36). The minimum corresponds to the vanishing variation $\delta\mathcal{L} = 0$. Performing the standard variational procedure and the integration by parts (taking into account that $\delta f(R) = 0$) we obtain the Euler-Lagrange equation (see, e. g., [6, 7])

$$\frac{\partial F}{\partial f} - \frac{d}{dr}\left(\frac{\partial F}{\partial f'}\right) = 0 \qquad (38)$$

for the integrand function in (37)

$$F(r, f, f') = \left(\sqrt{1+f'^2} + \lambda f(r)\right) r \,. \qquad (39)$$

Inserting (39) into (38), we obtain an easily solvable equation for $f(r)$, which yields

$$f(r, R) = \frac{1}{\lambda}\left(\sqrt{4-\lambda^2 r^2} - \sqrt{4-\lambda^2 R^2}\right) \,, \qquad (40)$$

where $f(r, R)$ is the function $f(r)$ at a given R. It corresponds to the liquid surface, represented by a segment of sphere with curvature radius $\bar{R} = 2/\mid\lambda\mid$. Besides, the surface is curved up for $\lambda > 0$ and down – for $\lambda < 0$. The parameter λ plays a similar role as f_0 in the model B. Eqs. (20) – (24), as well as (26) remain true in this case, whereas (25) has to be replaced by the relation where the increment $df(r, R)$ is expressed in terms of the increments $d\lambda$ and dR according to (40). Using these relations, it is straightforward to derive the differential equations for H and λ depending on R. The initial value of λ is found from the same consideration of the volumes as in model B. We have found it convenient to use the variable

$$y = \frac{\lambda R}{2} \qquad (41)$$

instead of λ in the final expressions. Note that $\mid y \mid = R/\bar{R}$. In summary, our equations for H and y read

$$\frac{dH}{dR} = Q(y, R) \,, \qquad (42)$$

$$\frac{dy}{dR} = \frac{y}{R} - \frac{y^5 + y^4\sqrt{1-y^2}\,\mathcal{B}(y, R)}{R\left(2 - 2\sqrt{1-y^2} - y^2\right)} \qquad (43)$$

where

$$\mathcal{B}(y, R) = (1-\mu)Q(y, R) + \frac{2\mu}{R^2}\int_0^R \frac{\partial h(r, R)}{\partial R} r dr \qquad (44)$$

and

$$Q(y, R) = \tan\left\{\gamma(R) - \arctan\left(\frac{\tan(\gamma - \theta(y))}{1-\mu}\right)\right\} \qquad (45)$$

with

$$\gamma(R) = -\arctan\left(\left.\frac{\partial h(r, R)}{\partial r}\right|_{r=R}\right) \qquad (46)$$

$$\theta(y) = -\arctan\left(\frac{y}{\sqrt{1-y^2}}\right) \,. \qquad (47)$$

The initial conditions are $H(R_0) = 0$ and $y(R_0) = y_0$, where y_0 is the real root of the equation

$$\frac{1}{3y^3}\left(1 - (1-y^2)^{3/2}\right) - \frac{\sqrt{1-y^2}}{2y} + \frac{\mu}{R_0^3}\int_0^{R_0} h(r, R_0) r dr = 0 \qquad (48)$$

within $-1 < y_0 < 0$. Since the expression in (48) represents a monotonous function of y in this interval, the root can be easily found by the Newton's iterations.

The numerical solution of (43) has some peculiarity in the vicinity of $y = 0$, since the denominator vanishes at $y \to 0$ according to

$$2 - 2\sqrt{1-y^2} - y^2 = \frac{y^4}{4} + O\left(y^6\right) \,. \qquad (49)$$

ISBN: 978-960-474-268-4

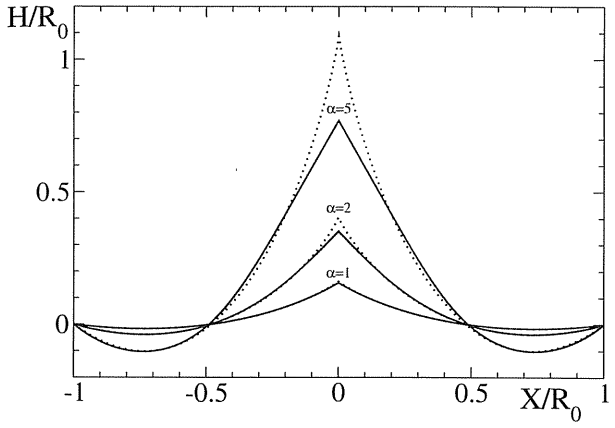

Figure 4: The profile (crossection) of the surface structure after the solidification for various values of the parameter α. Solid lines show the results of model C, whereas dotted lines – those of model B.

It means that dy/dR cannot be numerically calculated from (43) with a satisfactory accuracy if $\mid y \mid$ is too small. The problem can be solved by representing (43) as

$$\frac{dy}{dR} = -\frac{3y + 4\mathcal{B}(y,R)}{R} + O\left(y^2\right) \qquad (50)$$

for $\mid y \mid < \varepsilon$, where ε is an appropriately chosen small parameter. We have found the value 0.002 of ε to be nearly optimal in our example calculations by the fourth–order Runge–Kutta method, using a double–precision FORTRAN code. The integral relation (34), which holds also in model C, was satisfied with the numerical error of about $3 \cdot 10^{-10}$ in this case. The accuracy of such a method can be improved by adding expansion terms of higher orders in (50).

The spherical shape of the liquid surface (40) can be well approximated by the parabolic one (19) at small $\mid \lambda \mid$ (small $\mid y \mid$) or for a relatively flat surface. In this case we have $y \simeq 2f_0/R$, and Eq. (50) reduces to the one for f_0 (27).

The calculation results, taking the same examples for the parabolic solid–liquid interface as in Sec. 3.2, are shown in Fig. 4. The comparison between the model B and model C shows that the formed surface profile is less sharp in its central part for the model C. The difference increases with α, since the liquid surface becomes more curved, and therefore the parabolic approximation of model B less accurate in this case.

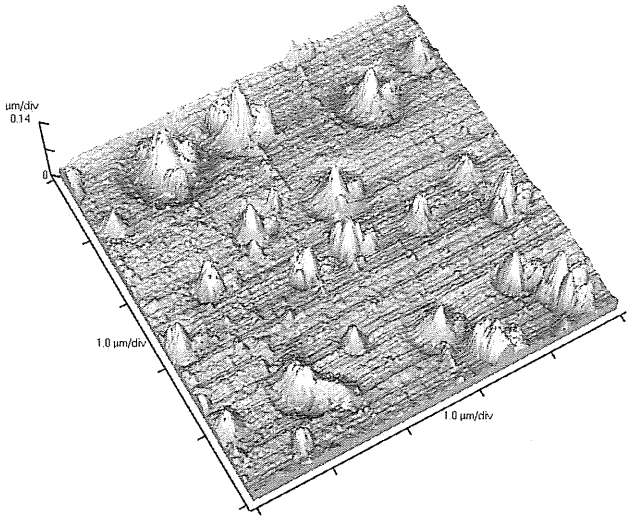

Figure 5: Surface topology of the Si-Ge sample after the laser treatment.

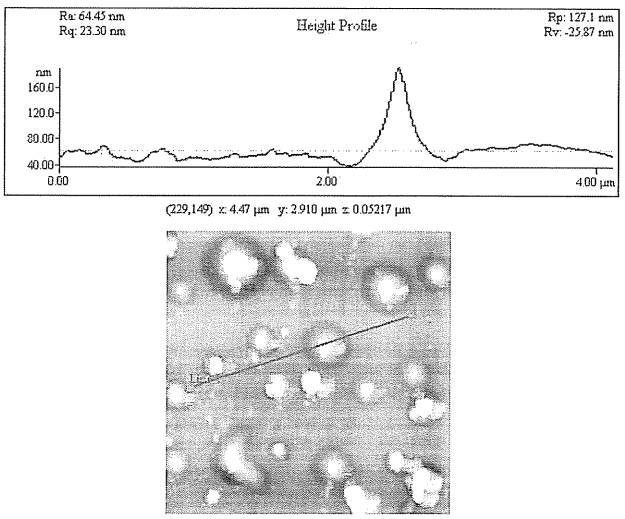

Figure 6: Surface profile of the Si-Ge sample after the laser treatment (top). The profile height is measured along the line indicated in the lower picture, showing the surface topology from above.

ISBN: 978-960-474-268-4

4 Comparison with experiments

We have compared our calculation results with the experimentally measured surface profile of $Si - Ge$ samples (with Ge as an impurity) after the laser irradiation, melting and solidification process. Besides, a nonuniform distribution of Ge has been reached in a preceding laser treatment, such that Ge concentrates in small islands on the surface of the sample.

Experiments were performed in ambient atmosphere at pressure of $1\,\mathrm{atm}$, $T = 20°C$ and 60% humidity. The structure of $Si_{1-x}Ge_x/Si$ solid solution with $x = 0.15$ has been treated with the radiation from a pulsed $Nd : YAG$ laser. The thickness of Si wafer was $300\,\mu\mathrm{m}$, whereas that of the $Si_{1-x}Ge_x$ layer was $500\,\mathrm{nm}$. The basic frequency with the following parameters: pulse duration $\tau = 15\,\mathrm{ns}$, wavelength $\lambda = 1.06\,\mu\mathrm{m}$, pulse rate $12.5\,\mathrm{Hz}$ and power $P = 1.0\,\mathrm{MW}$ was used. The second harmonic with $\tau = 10\,\mathrm{ns}$ and $\lambda = 532\,\mathrm{nm}$ was used for Si single crystals with SiO_2 cover layer. The spot of laser beam with $3\,\mathrm{mm}$ in diameter was scanned over the sample surface by a two coordinate manipulator in 1 and $2\,\mathrm{mm}$ steps. The surface morphology was studied by atomic force microscope (AFM).

At 15% concentration of Ge atoms, the formation of cones looks like "tree ring" growth [1] due to the melting of Ge separated islands on the irradiated surface at the laser beam intensity of $I = 20\,\mathrm{MW/cm^2}$. The melting and formation of certain surface structures after the solidification has been observed just in these local regions, as shown in Fig. 5. The shapes of the most of the impurity–islands were almost symmetric with relatively small deviations from the cylindric symmetry. The height of the surface profile, measured along the crossection of one such island, is shown in Fig. 6. As we see, the measured surface profile is very similar or qualitatively the same as in our calculations.

5 Conclusions

Three models (A, B and C), representing approximations of different levels, have been proposed for calculation of the surface structure formed in the solidification process after the laser irradiation. The model A ignores the curvature of the liquid surface, whereas the model B approximates its crossection by a parabola, which is a good approximation for relatively flat surfaces. The model C takes into account the real equilibrium shape of the liquid surface, which is found to be a segment of a sphere. The refined models (model B and model C) provide quite realistic shapes of the formed structures (Figs. 3, 4) in a qualitative agreement with the experimentally observed conic shapes of such structures – see Fig. 1 in [1] and Fig. 6 in this paper.

References:

[1] J. Eizenkop, I. Avrutsky and G. Auner, Single pulse excimer laser nanostructuring of thin silicon films: Nanosharp cones formation and heat transfer problem, *J. Appl. Phys.* 101, 2007, 094301.

[2] D. G. Georgiev, R. J. Baird, I. Avrutsky, G. Auner and G. Newaz, controllable excimer-laser fabrication of conical nano-tips on silicon thin films, *Appl. Phys. Lett.* 84, 2004, pp. 4881–4883.

[3] D. G. Georgiev, R. J. Baird, I. Avrutsky, J. Eizenkop, G. Auner and G. Newaz, *Spring Meeting of the Materials Research Society,* San Francisko, CA, April 2006, Symp. L, p. 252.

[4] G. B. Arfken and H. J. Weber, *Mathematical Methods for Physicists,* 6th ed., Academic Press, Orlando, FL 1985.

[5] J. D. Lambert and D. Lambert, *Numerical Methods for Ordinary Differential Systems. The Initial Value Problem,* Wiley, New York 1991.

[6] C. Lanczos, *The Variational Principles of Mechanics,* 4th ed., Dover, New York 1986.

[7] A. R. Forsyth, *Calculus of Variations,* Dover, New York 1960.

ISBN: 978-960-474-268-4